American Mineralogist, Volume 79, pages 615–621, 1994

High-pressure crystal chemistry of neighborite, $NaMgF_3$: An angle-dispersive diffraction study using monochromatic synchrotron X-radiation

YUSHENG ZHAO,* JOHN B. PARISE, YANBIN WANG, KEIJI KUSABA, MICHAEL T. VAUGHAN, DONALD J. WEIDNER

CHiPR and the Department of Earth and Space Sciences, State University of New York, Stony Brook, New York 11794-2100, U.S.A.

T. KIKEGAWA, J. CHEN, O. SHIMOMURA

Photon Factory, National Laboratory for High Energy Physics, Tsukuba, Ibaraki, 305, Japan

ABSTRACT

The crystal structure of neighborite ($NaMgF_3$) is determined at high pressure using monochromatic synchrotron X-ray powder diffraction data with Rietveld structural refinement methods. The previously assumed regularity of the MgF_6 octahedra at high pressure in the perovskite structure is demonstrated to be valid. The pressure-induced dimensional changes are expressed empirically as a combination of compression of the Mg-F bond length and tilting of the MgF_6 octahedral framework. We demonstrate that the dominant compression mechanism involves shortening of the octahedral Mg-F bond, which contributes about 80% to the overall compression, with the remaining 20% due to an increase in octahedral tilting. Linear compressibilities are consistent with single-crystal elasticity data, with the significant anisotropy observed being directly related to the tilting freedom of the octahedra along each axis of the unit cell.

INTRODUCTION

Members of the orthorhombic ABX_3 perovskite group (*Pbnm*, $Z = 4$), which includes $NaMgF_3$ and $MgSiO_3$, have structures that are distorted from the ideal cubic structure by two independent octahedral tilts, θ and ϕ (Fig. 1). The tilt θ is about one of the diad axes, $[110]_p$, of the BX_6 octahedron; this is equivalent to a tilt about the orthorhombic **b** axis in the *Pbnm* phase. The tilt ϕ is about the $[001]_p$ axis of the BX_6 octahedron and corresponds to tilting about the **c** axis. The subscript p refers to the pseudocubic structure of the high-symmetry prototype. The θ tilting causes the bending of the ⟨B-X-B⟩ angle and thus a shortening of a and c, whereas the ϕ tilt causes a shortening of a and b. On the basis of the assumption that the BX_6 octahedra are regular, the unit-cell volume of a centrosymmetrically distorted ABX_3 perovskite with a space group of *Pbnm* can be readily written according to the formalism of O'Keeffe and Hyde (1977):

$$V = abc = 32[\text{B-X}]^3\cos^2\Phi \qquad (1)$$

where B-X is the bond length within the BX_6 octahedron and Φ is the tilting about the pseudo-threefold axis of the octahedra (Fig. 1). The quantitative relationship between the angles θ, ϕ, and Φ can be found in Zhao et al. (1993a, 1993b).

The pressure- and temperature-induced dimensional change of the perovskite structure can be decoupled into two constituent parts: (1) the compression or expansion of the octahedral bond length B-X and (2) the compression or expansion due to the BX_6 octahedral tilting, (Megaw, 1971; Hazen and Finger, 1982). Thus the volumetric expansion can be expressed as

$$\alpha_V = \alpha_{V0} + \alpha_{V\Phi} = \frac{3\partial[\text{B-X}]}{[\text{B-X}]\partial T} + \frac{2\partial\cos\Phi}{\cos\Phi\,\partial T} \qquad (2a)$$

and the volumetric compression as

$$\beta_V = \beta_{V0} + \beta_{V\Phi} = \frac{-3\partial[\text{B-X}]}{[\text{B-X}]\partial P} - \frac{2\partial\cos\Phi}{\cos\Phi\,\partial P}. \qquad (2b)$$

We have demonstrated that this structural model is applicable to the thermal expansion of many perovskite materials (Zhao and Weidner, 1991; Zhao et al., 1993a, 1993b). Further, our observations at high pressure suggested that the proposed model may also be applicable to the compression of the perovskite structure (Zhao et al., 1993c). Single-crystal elasticity data also support this conclusion (Zhao and Weidner, 1993). There were, however, two remaining problems related to our previous high-pressure compressional data. First, significant deviatoric stress existed during the cold-compression part of the experiment. Second, information on the octahedral tilting and the octahedral bond length were derived indirectly from the lattice parameters (O'Keeffe and Hyde, 1977). This approach uses the assumption that the octahedra remain regular under high-pressure conditions.

The present study is designed to obtain high-quality monochromatic diffraction data from powdered neigh-

* Present address: Seismological Laboratory, California Institute of Technology, Pasadena, California 91125, U.S.A.

0003–004X/94/0708–0615$02.00

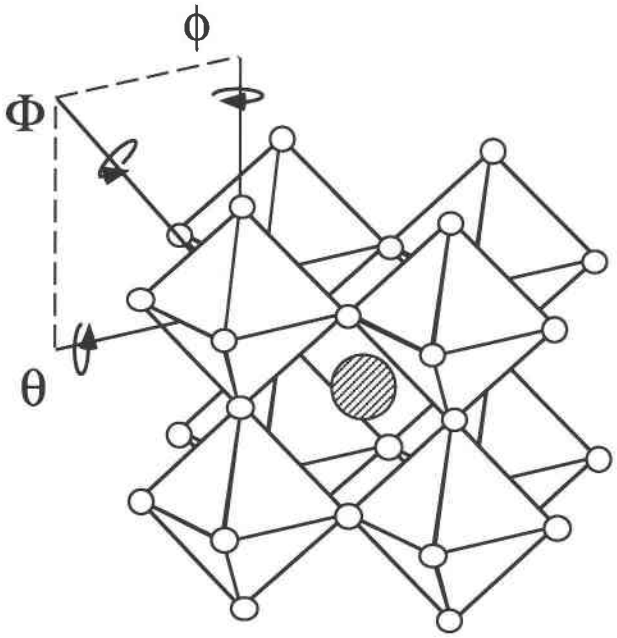

Fig. 1. The octahedral framework of an ideal cubic $Pm3m$ ABX_3 perovskite. The centrosymmetrically distorted orthorhombic perovskite with a space group of $Pbnm$ is derived through the combination of the octahedral rotation ϕ about $[001]_c$ and the octahedral tilting θ about $[110]_c$. It can also be conceived as the result of tilting Φ about the threefold $[111]_c$ axes of the regular octahedra.

borite under hydrostatic pressure conditions. By performing structural refinements, we can directly test the validity of published structural models for the compression mechanism. We also sought to evaluate the potential of a large volume apparatus for collecting powder diffraction data suitable for Rietveld refinement. It was hoped that the heating capabilities built into the DIA-6-type apparatus would alleviate the problem of strain broadening due to deviatoric stress at high pressure; this issue has dogged efforts to obtain sharp patterns in unheated high-pressure apparatus in the past.

Experimental methods

A powdered sample of the neighborite was synthesized following the method described by Chao et al. (1961). Stoichiometric proportions of NaF and MgF_2 were ground dry in an agate mortar. The mixture was sintered in a covered alumina crucible at 750 °C for 5 h. The resultant polycrystalline product had an X-ray diffraction pattern consistent with that published by Chao et al. (1961) and identical to the Rietveld refinement result of Zhao et al. (1993a).

High-pressure X-ray diffraction measurements were performed on the DIA-type cubic-anvil press (MAX-80) at the accumulator ring of the KEK, at the Tsukuba synchrotron radiation source (Shimomura et al., 1992). A portion of the sample was packed into a cylindrical amorphous-C furnace embedded in a boron-epoxy (BE) cube. A layer of NaCl powder, which serves as a pressure standard (Decker, 1971), was also packed into the sample chamber.

Before each data collection using monochromatic radiation, the instrument was operated in an energy-dispersive mode with white X-ray radiation to locate the sample position and to determine the cell pressure. The incident X-ray beam was collimated to 500 μm (width) $\times$ 200 μm (height). The energy-dispersive spectra were collected with a Ge solid-state detector at a fixed Bragg angle of $2\theta = 7.5°$ and displayed on a multichannel analyzer. The volumetric variation of the NaCl standard was determined from peak shifts, and the cell pressure was calibrated using the Decker (1971) equation of state.

The experiment was then switched to the angle-dispersive mode (Shimomura et al., 1992) to collect monochromatic synchrotron X-ray data at a wavelength of 0.3100(7) Å. The wavelength was selected using a double-bounce (Bragg-Bragg) monochromator assembly consisting of two Si_{111} crystals. The incident beam was decreased to 300 μm wide $\times$ 200 μm high, and a slit 300 $\times$ 100 μm was placed before the detector. With these beam optics, a peak full width at half maximum (FWHM) of ~0.05° is expected (Cox et al., 1988). The measured FWHM is actually ~0.06°, and with this resolution the peak-splitting of 200, 112, and 002 near $2\theta = 6.5°$ ($d \sim$ 2.7 Å) was clearly distinguished in the spectrum (Fig. 2).

Angle-dispersive data were collected from $4° > 2\theta > 16°$ in steps of 0.01°, with a counting time of 60 s per step. The average ring current was 30 mA at 6.5 GeV. Data were normalized by monitoring the incident beam using an Ar ionizing chamber. No correction was made for absorption.

Previous experience (Weidner et al., 1994) with a DIA-type apparatus indicates that deviatoric stress at high pressure tends to broaden diffraction peaks because of microstrain induced by grain-to-grain contact. The FWHM of the diffraction peaks of the powder sample of neighborite increases dramatically with increasing pressure and becomes saturated at pressures of about 3–4 GPa, where the deviatoric stress reaches the yield strength of the sample (Zhao et al., 1993c). Upon heating, the yield strength of the sample, and thus the FWHM of the diffraction peaks, decreases continuously, reproducing the ambient value at about 500 °C (Zhao et al., 1993c). This indicates a vanishing of the deviatoric stress. In the present study, following the initial data collection at room pressure and temperature, the cell assembly was first taken to high pressure and then heated to 600 °C for ½ h to ensure that sample compression was hydrostatic. Data collected at several places within the sample assured us that this treatment is effective in reducing the deviatoric stress to zero while not promoting significant grain growth. The pressure was then calibrated. The ability to remove stresses within the sample by annealing is a distinct advantage in this type of work.

The diffraction patterns of neighborite were analyzed using the Rietveld refinement technique (Rietveld, 1969) built into the generalized structure analysis system

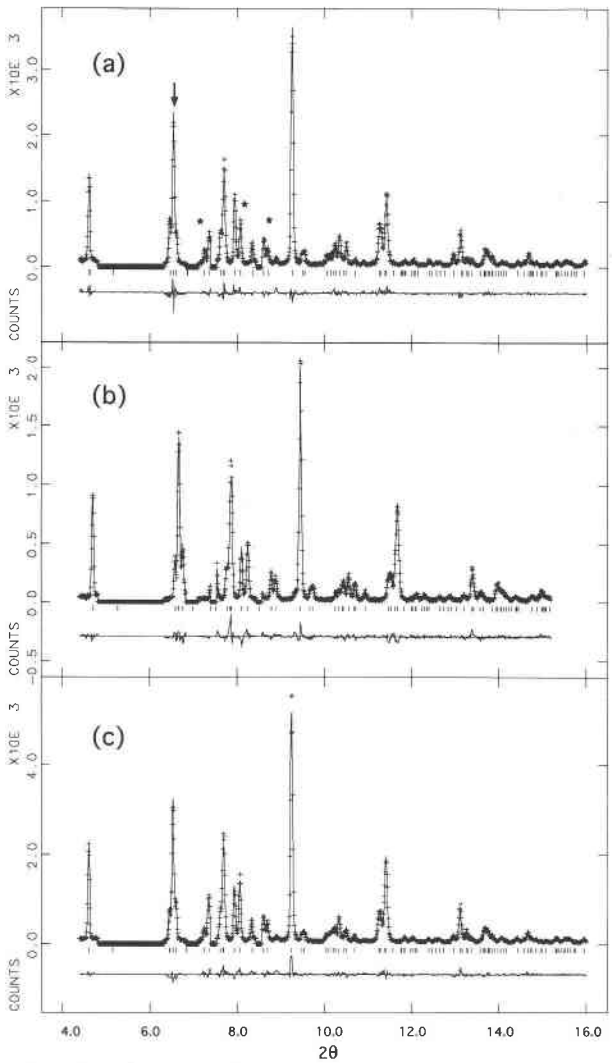

Fig. 2. The angle-dispersive synchrotron X-ray diffraction patterns of neighborite observed (**a**) at ambient conditions, (**b**) at $P = 4.9$ GPa, and (**c**) at ambient conditions after depressurization. Structural distortions and phase transitions can be monitored from the relative intensities of reflections and peak splitting resulting from the removal of symmetry elements from the $Pm3m$ perovskite substructure shown in Fig. 1. For example, a triplet of reflections associated with the orthorhombic distortion from the cubic substructure ($a \approx 3.8$ Å) to the $\sqrt{2}a \times \sqrt{2}a \times 2a$ superstructure is indicated by an arrow in **a**; in this case the distortion results in the cubic (110) reflection splitting into the orthorhombic (020), (112), and (200). Some of the low angle extra reflections, not associated with the cubic subcell, are also indicated with asterisks in **a**. Experimental data are shown as crosses, and the calculated profile is drawn as a continuous line. Tick marks below the patterns and above the difference curves are at positions of all possible reflections in the range of data.

(GSAS), distributed by Larson and Von Dreele (1988). A structure model previously refined using room-pressure data was used as a starting point. The results for the three data sets, collected before compression, at 4.9 GPa, and following decompression, quickly converged to the models summarized in Table 1. At low angles, the patterns contain some contaminant reflections from the cell assembly materials, magnesium oxide and boron nitride. The strongest of these has about 15% of the intensity of the largest perovskite reflection; the rest have <10%. Fortunately, only a few reflections from $NaMgF_3$ below 9° 2θ were affected. Those regions were excluded from the refinement (Fig. 2).

Table 1. Structural parameters refined* using powder-diffraction data collected in MAX-80 apparatus at ambient and high-pressure conditions

Atom**	P (GPa)	x	y	z	$U_{iso} \times 10^2$ (Å²)
Na	0.00	0.9851(9)	0.0455(8)	0.25	4.2(1)
	4.9	0.9824(9)	0.0473(10)	0.25	4.6(2)
	0.00	0.9860(7)	0.0422(7)	0.25	4.1(1)
Mg	0.00	0.0	0.5	0.0	2.6(1)
	4.9	0.0	0.5	0.0	3.4(2)
	0.00	0.0	0.5	0.0	3.1(1)
F1	0.00	0.088(1)	0.474(1)	0.25	3.3(2)
	4.9	0.097(1)	0.469(1)	0.25	4.0(2)
	0.00	0.0912(8)	0.4711(8)	0.25	3.5(2)
F2	0.00	0.7022(6)	0.2946(6)	0.0480(5)	3.2(2)
	4.9	0.7006(6)	0.2970(7)	0.0498(6)	3.1(1)
	0.00	0.7052(4)	0.2943(5)	0.0455(5)	2.7(1)

* The three entries for each set of parameters refer to the data collected in MAX-80 under ambient conditions at room pressure (top rows), at 4.9 GPa (middle rows), and from the decompressed sample at room pressure (bottom rows). Final agreement factors and cell parameters for the three refinements are $R_{wp} = 11.83$, $R_p = 8.27\%$, $R_N = 4.76\%$, $\chi^2 = 2.61$, $a = 5.3603(7)$, $b = 5.4884(7)$, $c = 7.666(1)$ Å at initial room pressure; $R_{wp} = 12.89\%$, $R_p = 9.26\%$, $R_N = 3.94\%$, $\chi^2 = 2.03$, $a = 5.2386(5)$, $b = 5.3796(6)$, $c = 7.5052(9)$ Å at 4.9 GPa; and $R_{wp} = 11.83\%$, $R_p = 8.29\%$, $R_N = 4.83\%$, $\chi^2 = 2.64$, $a = 5.3609(8)$, $b = 5.4828(8)$, $c = 7.667(1)$ Å at room pressure following decompression.

** Space group *Pbnm*.

Interestingly, although there is no indication of preferred orientation in the uncompressed sample, both the 4.9-GPa and room-pressure data collected after decompression show this effect. The consequences of this observation are discussed below.

Analysis of the compression mechanism

The overall volumetric compression of the orthorhombic *Pbnm* phase of neighborite at 4.9 GPa was determined to be 6.3%. The *a*, *b*, and *c* dimensions of the unit cell are compressed by 2.3, 2.0, and 2.1%, respectively.

TABLE 2. Selected interatomic distances (Å) and angles (°)

Atoms	0 Gpa (before)	4.9 GPa	0 Gpa (after)
Na-F1	3.187(6)	3.166(9)	3.182(6)
Na-F1	2.414(6)	2.349(9)	2.418(6)
Na-F1	3.098(8)	3.063(8)	3.119(6)
Na-F1	2.321(8)	2.244(7)	2.299(6)
Na-F2 × 2	2.563(5)	2.498(6)	2.576(4)
Na-F2 × 2	2.302(5)	2.234(6)	2.315(5)
Na-F2 × 2	2.710(5)	2.659(6)	2.705(4)
Na-F2 × 2	3.393(5)	3.354(5)	3.358(4)
Mg-F1 × 2	1.979(1)	1.950(1)	1.985(1)
Mg-F2 × 2	1.988(3)	1.947(3)	1.973(2)
Mg-F2 × 2	1.981(3)	1.948(4)	1.984(3)
F1-Mg-F1	180	180	180
F1-Mg-F2 × 2	88.3(2)	88.7(2)	88.9(2)
F1-Mg-F2 × 2	90.6(2)	91.4(2)	91.8(2)
F1-Mg-F2 × 2	91.7(2)	91.3(2)	91.1(2)
F1-Mg-F2 × 2	89.4(2)	88.6(2)	88.2(2)
F2-Mg-F2 × 2	89.37(6)	89.35(7)	89.41(5)
F2-Mg-F2 × 2	180	180	180
F2-Mg-F2 × 2	90.63(6)	90.65(7)	90.59(5)
F2-Mg-F2 × 2	180	179.97(2)	180
Mg-F1-Mg	151.1(3)	148.3(3)	150.0(2)
Mg-F2-Mg	150.1(2)	149.0(2)	151.4(2)

These results are in good agreement with the elastic bulk modulus of $K = 75.6$ GPa and the linear compressibilities of $\beta_a = 4.88 \times 10^{-3}$/GPa, $\beta_b = 3.90 \times 10^{-3}$/GPa, and $\beta_c = 4.29 \times 10^{-3}$/GPa, as derived from single-crystal elasticity data (Zhao and Weidner, 1993). This is also consistent with our previous high-pressure experiments in which significant anisotropy in the linear compressibilities, $\beta_a > \beta_c > \beta_b$, was observed (Zhao et al., 1993c).

Selected interatomic distances and angles for the NaF_{12} dodecahedron and the MgF_6 octahedron are listed in Table 2. The octahedral tilts of θ, ϕ, and Φ and the mean octahedral Mg-F bond length (see Appendix 1 in Zhao et al., 1993a) are given in Table 3. One can readily identify that the relative changes in the octahedral tilts are in the order: $(\partial \cos \Phi)/\cos \Phi > (\partial \cos \theta)/\cos \theta > (\partial \cos \phi)/\cos \phi$. Such an order is directly related to the significant anisotropy observed in the linear compressibility of the perovskite structure, where

$$\beta_a = \beta_{[B\text{-}X]} + \beta_\Phi = \frac{\partial[B\text{-}X]}{[B\text{-}X]\partial P} + \frac{2\partial \cos \Phi}{\cos \Phi\, \partial P} \quad (3a)$$

$$\beta_b = \beta_{[B\text{-}X]} + \beta_\phi = \frac{\partial[B\text{-}X]}{[B\text{-}X]\partial P} + \frac{2\partial \cos \phi}{\cos \phi\, \partial P} \quad (3b)$$

$$\beta_c = \beta_{[B\text{-}X]} + \beta_\theta = \frac{\partial[B\text{-}X]}{[B\text{-}X]\partial P} + \frac{2\partial \cos \theta}{\cos \theta\, \partial P}. \quad (3c)$$

The observed significant anisotropy in linear compressibility reflects that more degrees of freedom in octahedral tilting affect the a cell parameter of the orthorhombic (*Pbnm*) perovskite than affect the c and b (see Zhao et al., 1993a). One can also calculate the relative contribution of octahedral tilting and octahedral bond length to the overall volumetric compression of the neighborite by applying Equation 2b. It was determined that the compression of the octahedral Mg-F bond length, [Mg-F], is $\delta V_0/V_0 = 3\delta$[Mg-F]/[Mg-F] = 5.06%, which accounts for about 80% of the overall volumetric compression, whereas the

TABLE 3. Octahedral tilt angles (°) and bond lengths (Å) derived from the structural refinements

	0 Gpa (before)	4.9 GPa	0 Gpa (after)
$\theta[110]_p$	14.5(2)	15.9(2)	15.0(1)
$\phi[001]_p$	10.9(1)	10.7(1)	9.9(1)
$\Phi[111]_p$	18.1(2)	19.1(2)	17.8(2)
$[Mg\text{-}F]_m$	1.983	1.948	1.981

octahedral tilting $\delta V_\Phi/V_\Phi = (2\delta \cos \Phi)/\cos \Phi = 1.32\%$, which contributes only about 20% to the overall volumetric compression. This estimation agrees remarkably well with the values derived from single-crystal elastic compliances (Zhao and Weidner, 1993). It also demonstrates that our previous estimation of structural distortion based on lattice parameters observed at high pressures is justified. Zhao et al. (1993a) defined an octahedral strain, e_{ij}^{oct}, to describe the distortion of the octahedra, i.e.,

$$e_{ij}^{oct} = \begin{cases} \delta[B\text{-}X_i]/[B\text{-}X]_m & i = j \\ \pi/2 - \langle X_i\text{-}B\text{-}X_j \rangle & i \neq j \end{cases} \quad (4)$$

where $[B\text{-}X]_m$ is the mean octahedral bond length, $\delta[B\text{-}X_i]$ is the deviation of individual bond lengths from the mean, and $\langle X_i\text{-}B\text{-}X_j \rangle$ is the angle in radians between two octahedral bonds. The magnitude of e_{ij}^{oct} is calculated as

$$|e^{oct}| = \sqrt{\sum (e_{ij}^{oct})^2}. \quad (5)$$

From the structure refinement data (Table 2), we have derived the following octahedral strain values: Before compression, $|e^{oct}| = 0.0335$, at 4.9 GPa, $|e^{oct}| = 0.0355$, and following decompression, $|e^{oct}| = 0.0385$. These values are virtually the same and small, implying that assumptions of regularity of the octahedra at high pressure made by Zhao et al. (1993c) were reasonable.

FERROELASTIC TRANSITION

The structural distortion observed in the neighborite can be characterized by the spontaneous strain, which is equivalent to the macroscopic thermodynamic order parameter often applied to characterize the ferroelasticity of the crystal (Aizu, 1970). It has been demonstrated that the magnitude of spontaneous strain for the ferroic species, *m3mFmmm*, which includes neighborite, can be related to the lattice parameters (Zhao et al., 1993).

$$\epsilon_s\,(m3mFmmm) = \sqrt{\frac{2}{3}\left[\frac{(a+b)/2\sqrt{2} - c/2}{a_0}\right]^2 + 2\left(\frac{a-b}{2\sqrt{2}a_0}\right)^2}. \quad (6)$$

Here a, b, and c are the lattice parameters referred to the orthorhombic $Z = 4$ cell, and a_0 is the lattice parameter of the cubic prototype. The spontaneous strain is derived as $\epsilon_s = 0.0167$ at ambient conditions, $\epsilon_s = 0.0188$ at $P = 4.9$ GPa, and $\epsilon_s = 0.0159$ after decompression. The spontaneous strain, and hence the structural distortion of the perovskite, is increased by 11% by increasing the hydrostatic pressure to 4.9 GPa. This observation is quite dif-

ferent from those of previous experiments in which samples were compressed to 4.0 GPa but without being heated (Zhao et al., 1993c). In those cases the spontaneous strain was increased by 100%. Our new observations support the conclusion of Zhao et al. (1993c) that the doubling in spontaneous strain is mostly caused by deviatoric stress applied to the sample. The effect of hydrostatic pressure on the spontaneous strain is also compatible with the values derived from single-crystal elastic compliance data.

Another interesting observation in the present experiment concerns the ratios of intensities, such as I_{200}/I_{020}, I_{210}/I_{120}, I_{202}/I_{022}, I_{212}/I_{122}, . . . , I_{204}/I_{024}, and I_{400}/I_{040}. These were significantly increased during cold compression (see Fig. 2a, 2b). This phenomenon was retained in the diffraction spectrum after the annealing treatment of the sample and also after the total release of pressure. The Rietveld refinement result showed that this relative change in intensity resulted largely from a preferred orientation effect of about 20%.

This preferred orientation can be explained by twinning in the orthorhombic perovskite crystals (Abrahams, 1971; Salje, 1990), indicative of a transition between ferroelastic orientation states within a single phase. That is distinct from a ferroelastic phase transition, in which the structure of the crystal is changing (Wadhawan, 1982). The {110} twinning in particular results in an interchange of the **a** and **b** axes between adjacent twin domains (Sapriel, 1975; Toledano and Toledano, 1980). This type of twinning was observed in virtually all the *Pbnm* perovskites (Wang et al., 1992) and can be produced either by phase transitions or by deformation. The geometry of the cell assembly used has a cylindrical symmetry, and previous studies have shown that the stress field of the sample is such that the principal stress, σ_1, parallel to the cylinder axis, is different from those perpendicular to the axis (Weidner et al., 1992). Thus, a deviatoric stress ($\sigma_1 - \sigma_3$) is present in the sample, subparallel to the diffraction vector. Under this deviatoric stress, the initially randomly oriented crystals became aligned by twinning during compression. The {110} twinning results in the switching of the **a** and **b** axes among the twin domains, giving rise to the observed preferred orientation in the diffraction pattern.

The preferred orientation, once established, cannot be eliminated upon removal of the deviatoric stress by annealing nor can it be removed by releasing the load on the sample, as long as the the deviatoric stress level remains low or does not reverse its sign. It can be inverted only through the changing of ferroelastic orientation states (i.e., twinning) by applying a deviatoric stress field in a direction opposite to that which originally created the preferred orientation.

Possible implications for the α_V and β_V of silicate perovskite

Physical properties of the perovskite materials depend very much on their crystal structure (Salje, 1989). Neighborite is isostructural and isoelectronic to the $MgSiO_3$ perovskite (Chao et al., 1961; O'Keeffe et al., 1979). The

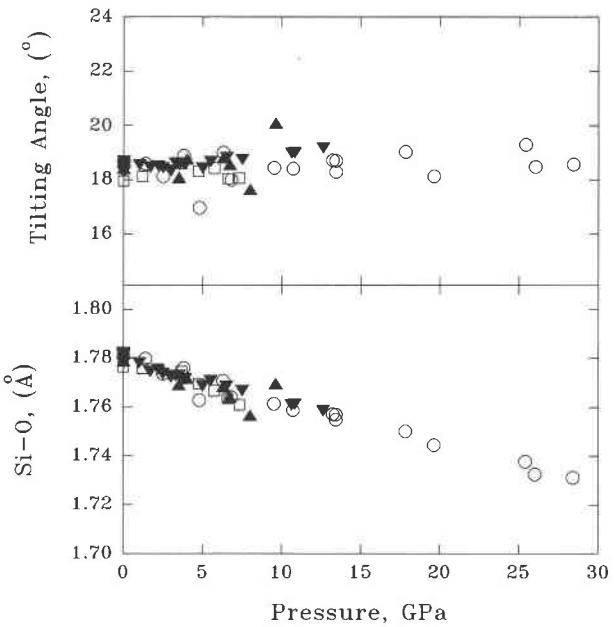

Fig. 3. The octahedral tilting angle Φ and the octahedral Si-O bond length of the silicate perovskites as derived from lattice parameters (see Zhao et al., 1993a) are plotted as a function of pressure. The diagram shows that the compression of the $MgSiO_3$ perovskite structure is mostly (~70%) accomplished by compression of the SiO_6 octahedra, whereas the octahedral tilting accounts for about 30% of the overall volumetric compression. The open symbols indicate data derived from Wang et al. (1991, 1994: squares) and Mao et al. (1991: circles). The solid symbols show the single-crystal data from Kudoh et al. (1987: triangles pointing up) and Ross and Hazen (1990: triangles pointing down).

comparable ionic radii and the 1:2 electronic charge ratio for ions make neighborite an ideal analogue for silicate perovskite. The weaker bonding strength of the fluoride perovskite allows us to simulate the ultrahigh-pressure and -temperature behaviors of the silicate perovskite at relatively lower pressures and temperatures (O'Keeffe et al., 1979). The structural model of thermal expansion and compression demonstrated in the case of neighborite can also be applied to the $MgSiO_3$ perovskite.

Many experimental data on the compression and thermal expansion of $MgSiO_3$ perovskite have been collected in the past decade (Yagi et al., 1982; Knittle et al., 1986; Knittle and Jeanloz, 1987; Kudoh et al., 1987; Ross and Hazen, 1989, 1990; Wang et al., 1990; Parise et al., 1990; Mao et al., 1991). We can thus derive structural information on octahedral tilting and octahedral bond length from the unit-cell dimensions of $MgSiO_3$ perovskite (Zhao et al., 1993a), assuming regular SiO_6 octahedra throughout the perovskite structure. It is found that the response of the crystal structures of $MgSiO_3$ perovskites to pressure is quite different from their response to temperature. Plotted in Figures 3 and 4 are the structural data of tilting angle and bond length as functions of pressure and temperature. It is shown clearly in the diagrams that the compression of the $MgSiO_3$ perovskite structure is mostly

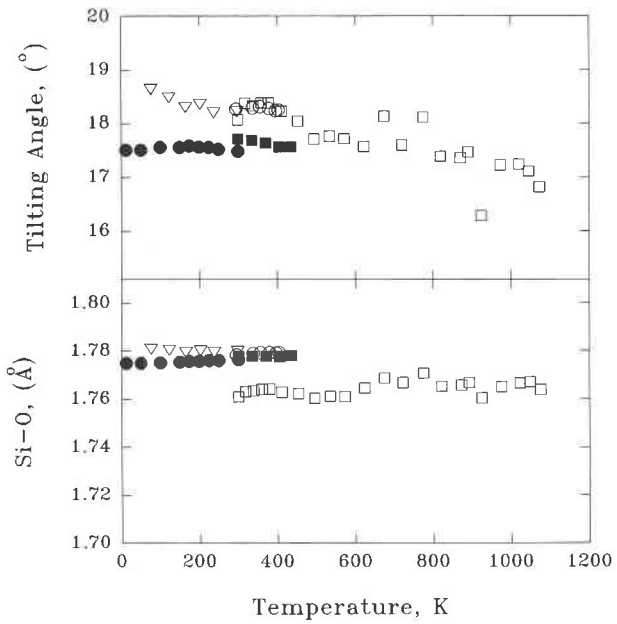

Fig. 4. The octahedral tilting angle Φ and the octahedral Si-O bond length of the silicate perovskites as derived from lattice parameters (see Zhao et al., 1993a) are plotted as a function of temperature for ambient pressure and for 7.3 GPa (Wang et al., 1991: open squares). The diagram shows that the octahedral Si-O bond length changes little with temperature, and thermal expansion of the $MgSiO_3$ perovskite at atmospheric pressure is mostly attributed to octahedral tilting. Data are derived from Ross and Hazen (1989: triangles), Parise et al. (1990: solid squares), and Wang et al. (1991, 1994: circles). The open symbols indicate data for the $MgSiO_3$ end-member, and the solid symbols indicate data for $(Mg_{0.9},Fe_{0.1})SiO_3$ perovskite.

(~70%) accomplished by the compression of the SiO_6 octahedra (Fig. 3), whereas the octahedral tilting increases slightly with pressure and accounts for only about 30% of the overall volumetric compression. On the other hand, the octahedral Si-O bond shows little change with temperature, and the thermal expansion of $MgSiO_3$ perovskite is mostly driven by octahedral tilting (Fig. 4). These observations are analogous to those for neighborite.

There is about a 1% difference in both octahedral tilting and octahedral bond length for data derived from unit-cell dimensions and those observed in single-crystal structure refinements (Horiuchi et al., 1987; Kudoh et al., 1987; Ross and Hazen, 1990). One can readily demonstrate that this offset is caused by the irregularity of the octahedra, namely, the octahedral strain (Zhao et al., 1993a). However, the structural data derived from single-crystal refinement and those derived macroscopically from the lattice parameters show similar overall behavior with pressure and temperature. The experimental data of both neighborite and $MgSiO_3$ perovskite show that thermal expansion is mostly accommodated by the octahedral tilting, whereas the dominant compressional mechanism is the octahedral bond compression.

By applying the structural model (Equations 2 and 3) to the single-crystal elastic compliance data of the $MgSiO_3$ perovskite (Yeganeh-Haeri et al., 1989), one can also assess the individual contribution of the octahedral bond and octahedral tilting to the overall volumetric compression of the perovskite. This assessment is in good agreement with the high-pressure compressional data; the dominant compression mechanism for silicate perovskite is the compression of the octahedral Si-O bond length (Zhao et al., 1993c).

Conclusions and implications

Defining a complete description of the physical properties of materials as a function of temperature and pressure is indeed an onerous task. If the physical properties depend only on volume, where volume expresses the net effect of the P-T state of the material, then the equation of state is considerably simplified, and there is not such a great need to gather an extensive data base for all materials at varying pressure and temperature. Indeed, the Grüneisen equation of state is based on the assumption that the phonon eigen frequencies depend only on volume.

With the data presented in this paper, along with our previous studies of the crystal structure of neighborite, we conclude that this simple picture is invalid for this perovskite. Pressure and temperature have very distinctive effects on the crystal structure. Thus, if one increases pressure and temperature in such a way as to maintain a constant volume, one finds that the octahedra get smaller and the tilt angle is reduced. Since crystal structure is more fundamental than volume in defining physical properties, one would not necessarily expect constant physical properties at a constant volume. Perhaps the most profound manifestation of the phenomenon is the observation that $(\partial\alpha/\partial P)_T = 0$ for compression up to 12% of volume. Thus, the Anderson-Grüneisen parameter, δ, which is generally expected to be about 4, is instead 0. This study of neighborite suggests that we must be careful in estimating the physical properties of $MgSiO_3$ perovskite at any given conditions.

Acknowledgments

This paper is a contribution of the Mineral Physics Institute at Stony Brook (MPI publication no. 104). Data collection at the KEK, Tsukuba, Japan, was supported as part of that institution's general user program for 1992–1993. This work was made possible by funding for the SUNY Stony Brook–Tsukuba University collaboration program from the Japanese Department of Education. M.T.V. received support from the Japanese Ministry of Education. J.B.P. and D.J.W. acknowledge the support of the NSF through grants DMR-9024249 and EAR-8804087, respectively. The Center for High Pressure Research (CHiPR) is an NSF-funded Science and Technology Center.

References cited

Abrahams, S.C. (1971) Ferroelasticity. Materials Research Bulletin, 6, 881–890.

Aizu, K. (1970) Determination of the state parameters and formulation of spontaneous strain for ferroelastics. Journal of the Physical Society of Japan, 28, 706–716.

Chao, E.C.T., Evans, H., Skinner, B., and Milton, C. (1961) Neighborite,

$NaMgF_3$, a new mineral from the Green River Formation, South Ouray, Utah. American Mineralogist, 46, 379–393.

Cox, D.E., Toby, B.H., and Eddy, M.M. (1988) Acquisition of powder diffraction data with synchrotron radiation. Australian Journal of Physics, 41, 117–131.

Decker, D.L. (1971) High-pressure equation of state for NaCl, KCl and CsCl. Journal of Applied Physics, 42, 3239–3244.

Hazen, R.M., and Finger, L.W. (1982) Comparative crystal chemistry, temperature, pressure, composition and the variation of crystal structure, p. 115–164. Wiley, New York.

Horiuchi, H., Ito, E., and Weidner, D.J. (1987) Perovskite-type $MgSiO_3$, single-crystal X-ray diffraction study. American Mineralogist, 172, 357–360.

Knittle, E., and Jeanloz, R. (1987) Synthesis and equation of state of $(Mg,Fe)SiO_3$ perovskite to over 100 gigapascals. Science, 235, 668–670.

Knittle, E., Jeanloz, R., and Smith, G.L. (1986) Thermal expansion of silicate perovskite and stratification of the Earth's mantle. Nature, 319, 214–216.

Kudoh, Y., Ito, E., and Takeda, H. (1987) Effect of pressure on the crystal structure of perovskite-type $MgSiO_3$. Physics and Chemistry of Minerals, 14, 350–354.

Larson, A.C., and Von Dreele, R.B. (1988) GSAS: Generalized structure analysis system. Los Alamos National Laboratory Report LAUR 86-748.

Mao, H.K., Hemley, R.J., Fei, Y., Shu, J.F., Chen, L.C., Jephcoat, A.P., Wu, Y., and Bassett, W.A. (1991) Effect of pressure, temperature and composition of lattice parameters and density of $(Fe,Mg)SiO_3$ perovskite to 30 GPa. Journal of Geophysical Research, 96, 8069–8079.

Megaw, H.D. (1971) Crystal structures and thermal expansion. Materials Research Bulletin, 6, 1007–1018.

O'Keeffe, M., and Hyde, B.G. (1977) Some structures topologically related to cubic perovskite (E21), ReO_3 (D09) and Cu_3Au (L12). Acta Crystallographica, B33, 3802–3813.

O'Keeffe, M., Hyde, B.G., and Bovin, J.-O. (1979) Contribution to the crystal chemistry of orthorhombic perovskite, $MgSiO_3$ and $NaMgF_3$. Physics and Chemistry of Minerals, 4, 299–305.

Parise, J.B., Wang, Y., and Yaganeh-Haeri, A. (1990) Crystal structure and thermal expansion of $(Mg,Fe)SiO_3$ perovskite. Geophysical Research Letters, 17, 2089–2092.

Rietveld, H.M. (1969) A profile refinement method for nuclear and magnetic structures. Journal of Applied Crystallography, 2, 65–71.

Ross, N.L., and Hazen, R.M. (1989) Single crystal X-ray diffraction study of $MgSiO_3$ perovskite from 77 to 400 K. Physics and Chemistry of Minerals, 16, 415–420.

——— (1990) High-pressure crystal chemistry of $MgSiO_3$ perovskite. Physics and Chemistry of Minerals, 17, 228–237.

Salje, E. (1989) Characteristics of perovskite-related materials. Philosophical Transactions of the Royal Society of London, A328, 409–416.

——— (1990) Phase transition in ferroelastic and co-elastic crystals, 366 p. Cambridge University Press, Cambridge, U.K.

Sapriel, J. (1975) Domain-wall orientations in ferroelastics. Physical Review B, 12, 5128–5140.

Shimomura, O., Utsumi, W., Taniguchi, T., Kikegawa, T., and Nagashima, T. (1992) A new high pressure and high temperature apparatus with sintered diamond anvils for synchrotron radiation use. In Y. Syono and M.H. Manghnani, Eds., High-pressure research: Application to Earth and planetary sciences, p. 3–11. Terrapub, Tokyo; American Geophysical Union, Washington, DC.

Toledano, J.-C., and Toledano, P. (1980) Order parameter symmetries and free-energy expansions for purely ferroelastic transitions. Physical Review B, 21, 1139–1172.

Wadhawan, V.K. (1982) Ferroelasticity and related properties of crystals. Phase Transitions, 3, 3–103.

Wang, Y., Guyot, F., Yeganeh-Haeri, A., and Liebermann, R.L. (1990) Twinning in $MgSiO_3$ perovskite. Science, 248, 468–471.

Wang, Y., Weidner, D.J., Liebermann, R.L., Liu, X., Ko, J., Vaughan, M.T., Zhao, Y., Yeganeh-Haeri, A., and Pacalo, R.E.G. (1991) Phase transition and thermal expansion of perovskite. Science, 251, 410–413.

Wang, Y., Guyot, F., and Liebermann, R.C. (1992) Electron microscopy of $(Mg,Fe)SiO_3$ perovskite: Evidence for structural phase transitions and implications for the lower mantle. Journal of Geophysical Research, 97, 12327–12347.

Wang, Y., Weidner, D.J., Liebermann, R.C., and Zhao, Y. (1994) *P-V-T* equation of state of $(Mg,Fe)SiO_3$ perovskite: Constraints on composition of the lower mantle. Physics of the Earth and Planetary Interiors, 83, 13–40.

Weidner, D.J., Wang, Y., and Vaughan, M.T. (1994) Yield strength at high pressure and temperature. Geophysical Research Letters, in press.

Yagi, T., Mao, H.K., and Bell, P.M. (1982) Hydrostatic compression of perovskite-type $MgSiO_3$. In S.K. Saxena, Ed., Advances in physical geochemistry, p. 317–325. Springer-Verlag, New York.

Yeganeh-Haeri, A., Weidner, D.J., and Ito, E. (1989) Single-crystal elastic moduli of magnesium metasilicate perovskite. In A. Navrotsky and D. Weidner, Eds., Perovskite: A structure of great interest to geophysics and material science. American Geophysical Union, Geophysical Monograph, 45, 13–35.

Zhao, Y., and Weidner, D.J. (1991) Thermal expansion of $SrZrO_3$ and $BaZrO_3$ perovskites. Physics and Chemistry of Minerals, 18, 294–301.

——— (1993) The single crystal elastic moduli of neighborite. Physics and Chemistry of Minerals, 20, 419–424.

Zhao, Y., Weidner, D.J., Parise, J.B., and Cox, D.E. (1993a) Structural distortion and thermal expansion of perovskite: Data for $NaMgF_3$ (I). Physics of the Earth and Planetary Interiors, 76, 1–16.

——— (1993b) Critical phenomena and phase transition of perovskite: Data for $NaMgF_3$ (II). Physics of the Earth and Planetary Interiors, 76, 17–34.

Zhao, Y., Weidner, D.J., Liebermann, R.L., Liu, X., Ko, J., Vaughan, M.T., Yeganeh-Haeri, A., and Pacalo, R.E.G. (1993c) Perovskite at high *P-T* conditions: An in-situ synchrotron X-ray diffraction study of $NaMgF_3$ perovskite. Journal of Geophysical Research, 99, 2871–2885.

MANUSCRIPT RECEIVED OCTOBER 19, 1993
MANUSCRIPT ACCEPTED MARCH 15, 1994